Bonding interface morphology of keyholeless friction stir spot welded joint of AZ31B Mg alloy and DP600 galvanized steel

Liu Xiao，Zhao Fengling，Niu Hongwei，Chen Yang，Wang Chenyang，Li Xiaoping

刘骁，赵凤玲，牛红伟，陈阳，王晨阳，李小平

Department of Materials Engineering, Jiangsu University of Technology, Changzhou 213100, China

Abstract   Because the bonding interface of dissimilar metal joint between AZ31B Mg alloy and DP600 galvanized steel by keyholeless friction stir spot welding (KFSSW) is permanent bonding, the interface morphology cannot be directly observed. If the joint is separated by external force, the original features of bonding interface of joint will be destroyed, which has influence on the accuracy for observation and analysis of the result. In this paper, the coordinates of the key point at the interface of every cross-section at intervals of 0.2 mm were measured and connected into an outline. The outline of all interfaces makes up the three-dimensional morphologies of bonding interface between AZ31B Mg alloy and DP600 steel by KFSSW, which was constructed by Solidworks software to restore the real mechanical bonding state of joint. Combined with the microhardness analysis of cross-section and results of in-situ tensile test, the unique bonding state and morphology of Mg and steel in the welded joint were confirmed.

Key words   keyholeless friction stir spot welding, Mg/steel, bonding interface morphology, microhardness, in-situ tensile

0　Introduction

In view of self-characteristics and massive weldings of Mg alloys and steel, their composite materials can partially replace steel structures in many engineering applications. This can effectively reduce the weight of structural parts, solve the problem of auto lightweight and provide feasible technical support for energy saving and environmental protection. Therefore, the welding of magnesium alloys and steel has attracted extensive attention from domestic and international scholars[1 – 4]. Keyholeless friction stir spot welding (KFSSW) is a solid-state welding technique with the merits of lower residual stress, minor distortion and keyhole-free joints, which is an ideal method of connecting dissimilar materials. Now KFSSW method is successfully applied to lap joint of Mg alloys and steel for effective bonding[5 – 12]. However, due to the complexity and instability of

KFSSW process of Mg alloys and steel, there is no clear interpretation of the bonding mechanism of Mg alloys and steel joint.

In this paper, Solidworks software is used to measure and draw the actual cross section coordinates of the joint, simulate the real shape of the joint bonding interface and conduct in-situ tensile test and section microhardness test on the joint. The purpose of above works is to provide a theoretical basis for researching the bonding mode of KFSSW joint between Mg and steel, and hopes to simulate real interface bonding morphology of the joint and provides ideas or helps for the scientific research on the need for non-destructive morphology restoration.

1　Material and method

1.1　Experimental materials

AZ31B Mg alloy plate of 2 mm thick and DP600 gal-

vanized steel plate of 1 mm thick were used in this study. The chemical compositions of two materials are shown in Table 1 and Table 2 respectively. The supply state of base metal is rolled state.

Table 1   Chemical compositions of AZ31B (wt. %)

| Element | Al | Zn | Mn | Si | Fe | Cu | Ni | Other elements | | Mg |
								Single	Total	
AZ31B	2.5–3.5	0.6–1.4	0.2–1.0	≤0.80	≤0.003	≤0.01	≤0.001	≤0.05	≤0.30	Balance

Table 2   Chemical compositions of DP600 (wt. %)

Element	C	Si	Mn	P	S	Al	N	Fe
DP600	0.079	1.00	1.52	0.015	0.005	0.023	0.003 7	Balance

1.2   Welding process parameters

A lot of experiments have found that the Mg plate would appear black, even burning, owing to serious oxidation, especially when the Mg plate was placed on the top of the steel. At the same time, considering the large difference of the melting point between Mg and steel, the materials directly contacting with the shoulder should choose the high melting point metal to ensure the utilization rate of heat generated by the rotating shoulder. Thus, all welds were made in a lap joint configuration with AZ31B on the bottom and DP600 on the top, as shown in Fig.1.
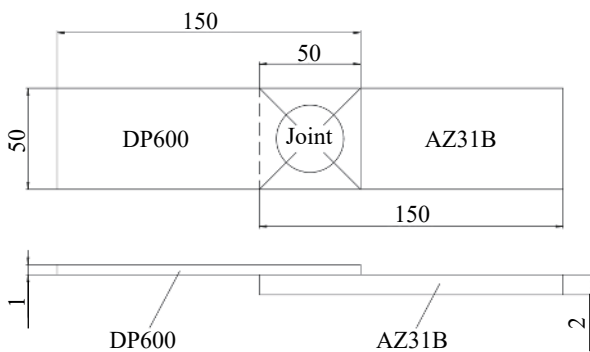
Fig. 1   The lap joint diagram of KFSSW(mm)

In this experiment the optimal process parameters, referred to the research results of other process parameters and combined with the experimental homework[13–17], were shown in Table 3.

The lap joints were obtained with the above process parameters and the macro-morphology of welding speci-men is shown in Fig. 2. The macro-morphology of the joint is shown in Fig. 3. The tensile shear tests of 6 joints showed that the average shear load of those joints was 9.3 kN.

1.3   Experimental method
1.3.1   Restoration of original interface morphology

The procedure of description and measurement of welded interface is shown in Fig. 4. First, the metallographic sample of whole joint was cut and fixed with resin. Then the cross-section of the sample was grinded and polished. The morphology of interface was measured and plotted by recording coordinates of the key point. Finally, the outline of interface was drawn according to all key point coordinates. The joint with a diameter of 20 mm was divided into 100 cross-sections. Two-dimensional outlines of interface of 100 cross-sections were sampled and fitted by Solidworks software to get three-dimensional interface morphology. Thus, the real morphology restoration of joint was realized.

1.3.2   Microhardness

The microhardness point starts at 0.25 mm from the boundary along the length direction and width direction of the cross-section of the joint, the interval of each point on all sides is also 0.25 mm. The loading pressure is 9.8 MPa and the holding time is 15 s. With this method, the hardness data of 350 points can be obtained in each cross-section. Hardness distribution of 6 cross-sections was respectively made by direct matrix transformation in Origin software. Interception of cross-section and position of microhardness points are shown in Fig. 5.

1.3.3   In situ tensile

The in-situ tensile specimen is obtained by cutting the

Table 3   Welding process parameters

Tool pin diameter/mm	Shoulder diameter/mm	Welding speed/(r.min⁻¹)	Shoulder plunge depth/mm	Pin length/mm
6	20	1 200	0.4	1.6

Fig. 2 Macro-morphology of joint by KFSSW
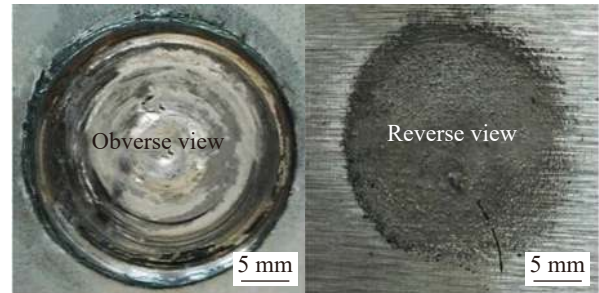
Fig. 3 Macro-morphology of the joint by KFSSW

Cross-section morphology

Marking coordinates of key points

Combination two-dimensional outlines

Generating two-dimensional outline
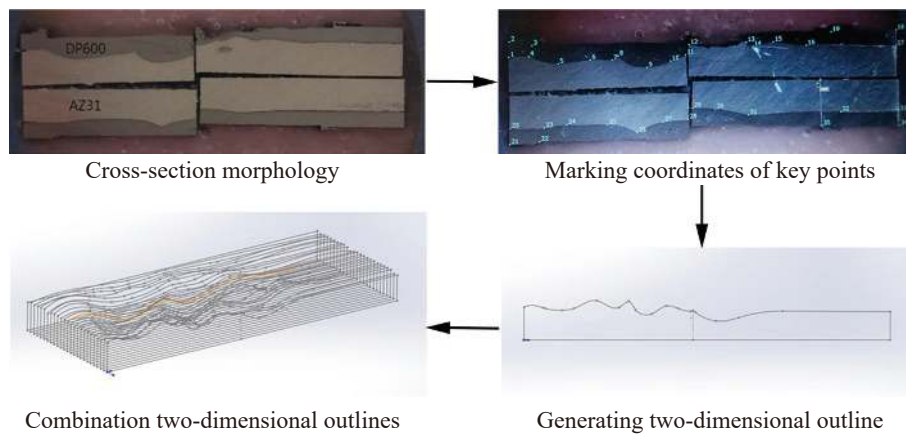
Fig. 4 Schematic diagram of restoration method of interface morphology

Get 6 cross profiles   350 microhardness points

X-X (A-A, B-B, C-C, D-D, E-E, F-F)
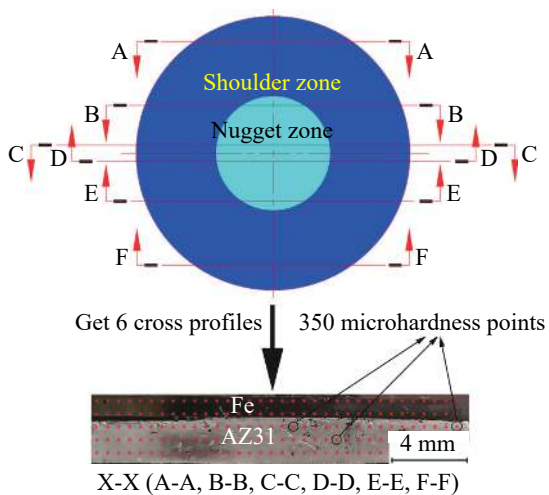
Fig. 5 Cross-section interception method and microhardness point position

sample along the center line of the welding spot, as shown in Fig. 6. The opening was cut along the edge of the welding spot on both sides of the Mg and steel surface to ensure that only the bonding interface is loaded during the in-situ tensile process. The surface of specimen was grinded and polished for observing the process of in-situ tensile test.
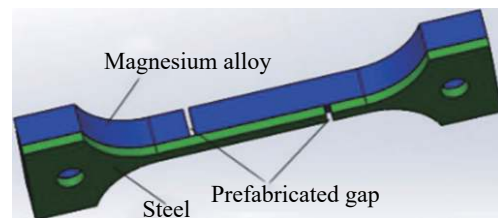
Fig. 6 Schematic diagram of in-situ tensile specimen

2 Results and discussion

2.1 Reappearance of bonding interface morphology of joint

As shown in Fig. 7, the three-dimensional interface morphology of all the cross-section coordinate outlines of joint on Mg side was obtained by the Solidworks software with lofting method and smooth transition. As shown in Fig. 8, The three-dimensional interface morphology of joint on DP600 steel side was also obtained by the same method.

The interface of Mg and steel were combined into a joint. The equiaxial view and lateral view of the joint are respectively shown in Fig. 9 and Fig. 10.
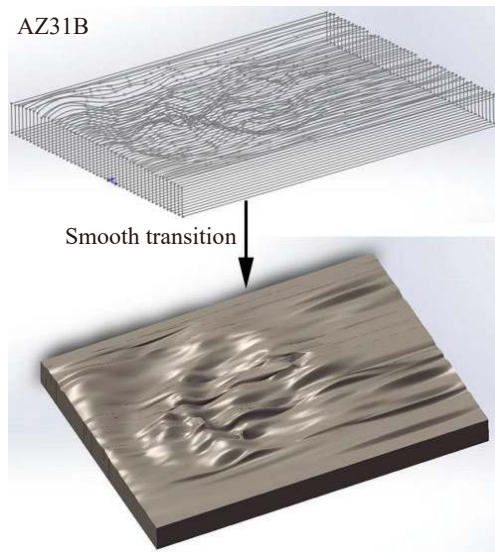
Fig. 7　Reappearance of surface morphology on the AZ31B side
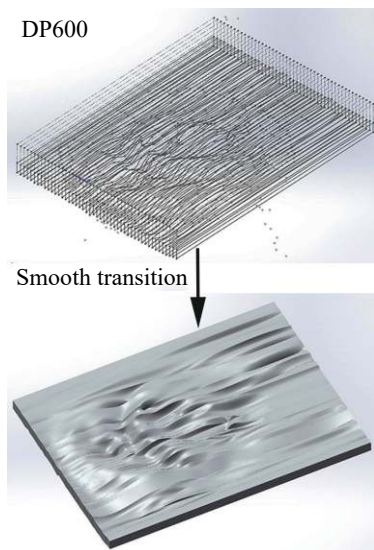
Fig. 8　Reappearance of surface morphology on the DP600 steel side
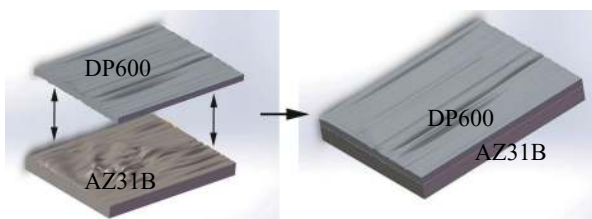
Fig. 9　Equiaxial view of joint between AZ31B Mg and DP600 steel by KFSSW
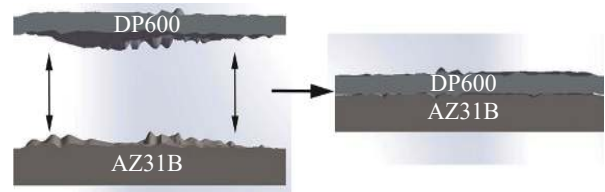
Fig. 10　Lateral view of joint between AZ31B Mg and DP600 steel by KFSSW

2.2　Analysis of bonding interface morphology of joint

Owing to the tightly integrated structure located in the bonding interface between AZ31B Mg and DP600 steel, the interface morphology characteristics between AZ31B Mg and DP600 steel were similar and mutual coupling. In order to convenient expression and analysis, this paper only studied the interface morphology characteristics on AZ31B Mg side and further reflect the interface characteristics of the entire joint.

Fig. 11 shows the interface morphology on AZ31B Mg side. A large number of nailed protuberances and sags were formed owing to the irregular plastic deformation of the AZ31B Mg plate and the plastic flow of the local metal under the effect of the severe squeeze from the stirring pin and the upset pressure from the shoulder. The deformation of AZ31B Mg was the most obvious and severe at the center area of joint under the effect of the pin. The wavy thermoplastic deformation of AZ31B Mg accompanied with the movement of the pin and shoulder. As shown in Fig. 11 a, the depth of the lowest wavy valley of AZ31B Mg was 1.53 mm, while the height of the highest nailed peak of AZ31B Mg was 2.93 mm, as shown in Fig. 11 b. Compared with 2 mm thick AZ31B Mg, the deformation degree was very intense.

Since the thickness of AZ31B Mg alloy plate is 2 mm and the thickness of DP600 galvanized steel plate is 1 mm, the thickness of joint was 3 mm. The thickness of steel plate covered on the AZ31Mg plate at the peak area only had 0.07 mm, as shown in Fig. 11 b. Because the position of the peak was the place of pin insertion, that was the starting welding position, the filling process of keyhole of joint during welding was further analyzed.

At the beginning position of welding, the steel plate was totally penetrated and crushed by the pin. The crushed steel particles at the keyhole position were extruded into the coverage area of the shoulder around the external circle of the pin. With the down pressure of shoulder, the movement of the tool and the retraction of pin, the steel particles distributed on the surface of the joint were again pushed back to the matrix. At the same time, the thermoplastic state of AZ31B Mg filled the position of the loss of steel. Because of the continuous extrusion of the shoulder, the Mg alloy
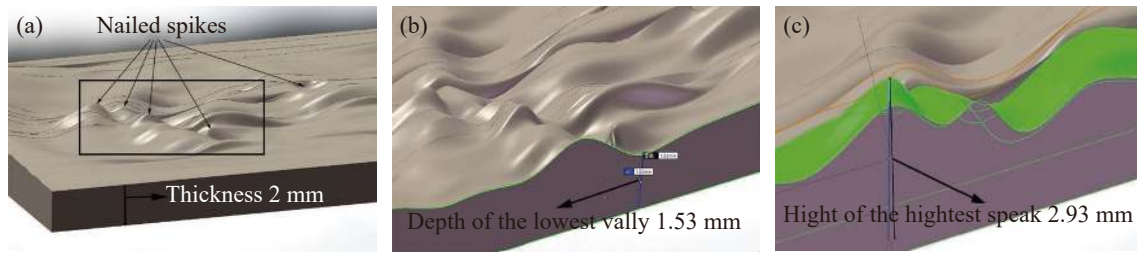
Fig. 11 Valley and peak at the AZ31B Mg interface (a) Interface morphology (b) Trough structure (c) Nail structure

filled in the holes of steel was tightly bonded with the steel matrix to form a firm mechanical bonding structure.

Although irregular wavy fluctuation appeared at the interface, it was found that the regularity characteristics by analyzing the overall interface are as follows.

(1) As shown in Fig. 12, there was a central area at the interface, where the wavy fluctuation was most obvious and intense. As shown in Fig. 11, valley and peak of wavy fluctuation also appeared the central area of the interface, similar to "hook", it can increase the strength of joint[18]. The area described above was the area of the effect of pin, which could be called stir zone. Due to the serious deformation at the interface, the mechanical bonding was most obvious, which ensured the bonding strength of the joint.
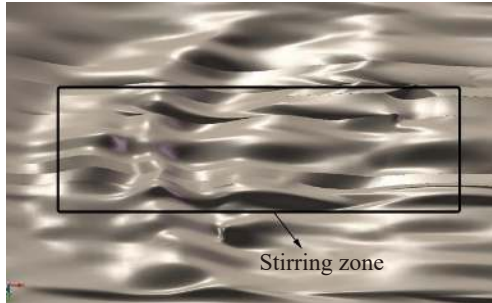
Fig. 12 Severe deformation in the stir zone

(2) As shown in Fig. 13, due to the extrusion effect of the shoulder, two ring indentations, which were equivalent to the shoulder area and similar to half-moon cave, were observed in the effect area of shoulder. In this position, the upper steel plate was integrally inlayed into the Mg alloy. The above structure will undoubtedly enhance the mechanical bonding strength of the joint. It is worth noting that this morphological feature cannot be found under the conventional analysis and observation method.

2.3   Analysis of cross-section morphology

The AZ31B Mg and DP600 steel were combined into a complete joint, and the cross-section specimen of the joint was cut along the X axis direction. According to the method shown in Fig. 14, taking the joint boundary as the starting
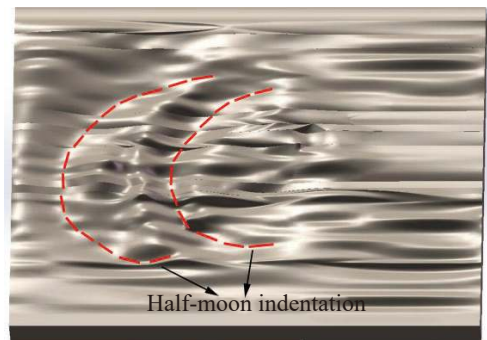
Fig. 13   Half-moon ring indentation in the shoulder effect zone
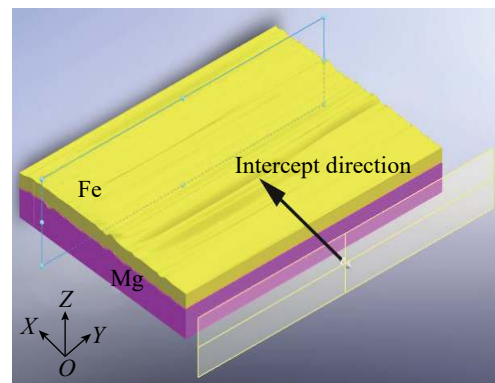
Fig. 14   Cross-section diagram along X axis direction

point, every cross-section morphology was intercepted at intervals of 1.5mm. The 15 cross-section morphologies of the joint are shown in Fig. 15. The serial number of the intercepted cross-section morphology is arranged according to the sequence number of a - o in Fig. 15.

The cross-section morphologies shown in Fig. 15 a– d were located at the shoulder area. Because this area was mainly squeezed by the shoulder accompanying with weak effect of the pin, the wave degree at the interface between Mg and steel was not obvious. With careful observation form cross-sections in Fig. 15 a–d, it was found that the degree of the interlaction and fluctuation at the interface appeared gradual increasing trend. Sharp wedge-shaped pro-
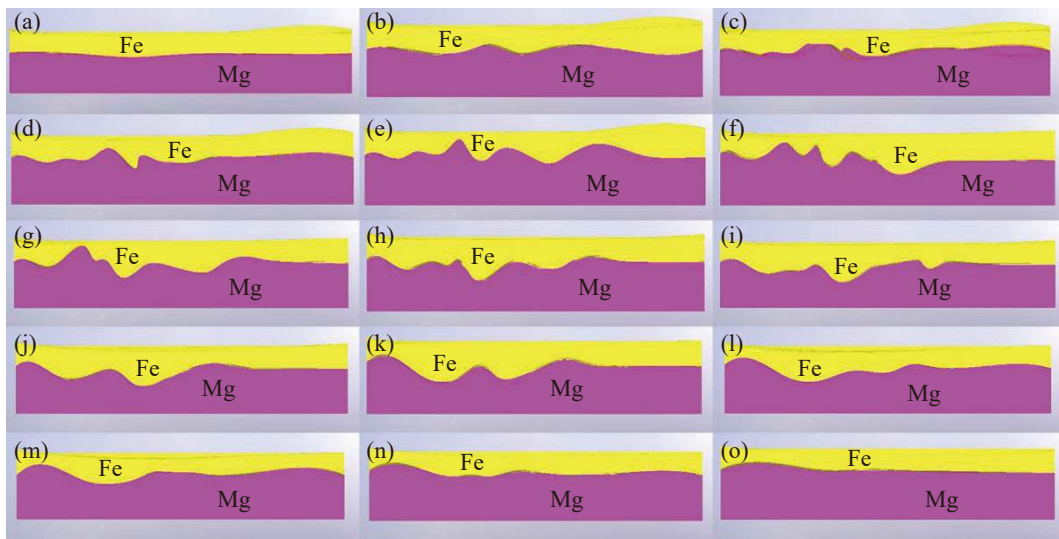
Fig. 15   **Cross-section morphologies of *X* axis direction**

tuberance was interlaced between Mg and steel can be observed in Fig. 15 d. It is speculated that the wedge-shaped protuberance not only ensure the close bonding of joint in the horizontal direction, but also still have a certain bonding force in the normal direction. The degree of interlaction and fluctuation shows a trend from weak to strong at the interface, which illustrates that the closer the center of the joint is, the more obvious the mechanical bonding is.

The cross-section morphologies shown in Fig. 15 e– f were located at the stirring area of joint. Because this zone was directly affected by the stir of pin, the mechanical bonding was most obvious. As shown in Fig. 15 e–f cross-section morphologies, the wave degree at the interface between Mg and steel was very sharp. The initial insertion position of the pin was the maximum peak of the deformation of Mg alloy appeared in the Fig. 15 e– f. Because the stirring pin started to weld in the left side of joint and moved to the right side with retraction of the pin, the peak of the wave appeared in the left side of the above cross-section morphologies, but the wave degree at the right side between Mg and steel was gentle. At the position of beginning welding, the insertion depth of the pin was the longest, so the left side of the cross-section morphologies appeared a large wave cluster after the deformation of Mg alloy. With the moving of the tool, the stirring pin gradually retracted from the inside of the workpiece, which weakened the stirring effect for Mg alloy and steel. So, the wave degree at the right side between Mg and steel was gentle.

The cross-section morphologies in Fig. 15 l–o were similar to the morphologies in Fig. 15 a–d. Away from the stirring zone, the wavy undulation at the interface between Mg and steel became more and more gentle with gradual weaken mechanical bonding.

According to the same method, the interception diagram

of the cross-section along *Y* axis direction is shown in Fig. 16 and the cross-section morphologies are shown in Fig. 17.
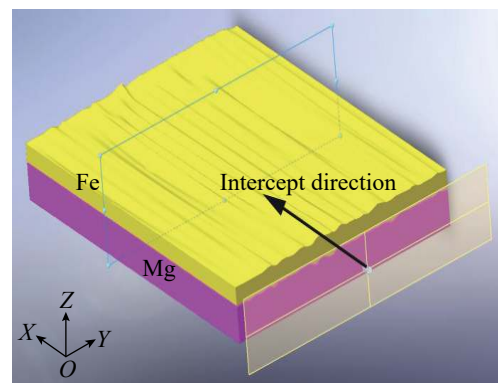
Fig. 16   **Cross-section diagram along *Y* axis direction**

The cross-section morphologies shown in Fig. 17 reflect the characteristics of different stages in the welding process. Observing all the morphologies in turn, it was found that Fig. 17 a was the cross-section morphology at the beginning of the welding and Fig. 17 n– o were the cross-section morphologies of the shoulder affected zone at the ending of the welding with no obvious mechanical bonding. The mechanical bonding characteristics were observed in Fig. 17 b–m and the trend of bonding characteristics from weak to strong was obvious. The above characteristics reflected three different stages of KFSSW process: the insertion stage of pin, the retraction stage of pin and the end stage of pin retraction. The characteristics of stirring effect were different from different stages, which can be reflected from the interface morphology of different zones. As the welding process proceeded, the stirring pin was gradually retracted, which made the stirring effect for workpiece
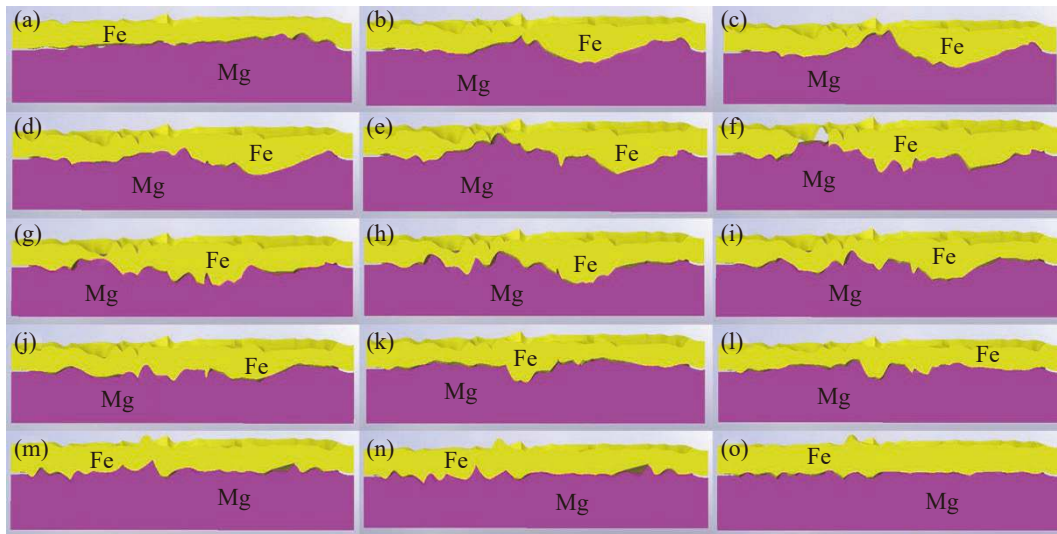
Fig. 17   **Cross-section morphologies of *Y* axis direction**

weaker and weaker, so the mechanical bonding effect was also worse and worse.

In order to verify the authenticity and accuracy of the restoration of entity morphology, the real cross-section morphologies of joint were shown in Fig. 18.
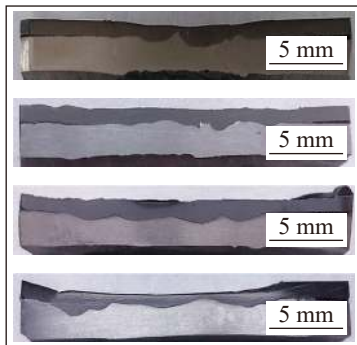
Fig. 18   **Real cross-section morphologies of joint**

By comparison and analysis of Fig. 15, 17 and 18, it could be seen that the experimental results in this paper were in agreement with the real joint characteristics. This further proves the authenticity and accuracy of the interface morphology of Mg/steel joint restored in this paper.

2.4   Analysis of microhardness

The hardness nephogram of 6 cross-sections was obtained, as shown in Fig. 19. The hardness of each base material was given, where AZ31B Mg alloy is 60 HV, DP600 galvanized steel is 130 HV, and the average hardness of the shoulder and pin is 300 HV. Fig. 19 a and fshows the hardness distribution of the affected zone of the shoulder. The severe plastic deformation of the steel plate was formed in this area under the directly effect of friction and extrusion of

the shoulder, which resulting in dislocation pile-up in the grain. The hardness of several small areas is as high as 207.5 HV, and the overall hardness is within the range of 148.4 HV–187.8 HV. The hardness distribution of joint is uneven and slightly higher than that of the parent material. The hardness of Mg alloy has little change. Mg is a close-packed hexagonal structure material, and the plastic deformation mode is mainly twin deformation, which requires greater shear stress. The extrusion of the shoulder is not enough to cause twin deformation of Mg alloy. Therefore, the dislocation density in the grain did not increase significantly and the hardness did not change significantly. Fig. 19 b shows the hardness distribution of the stirring zone. Compared with Fig. 19 a, the hardness is significantly increased. At the beginning of welding, the stirring pin penetrates the steel plate and is in direct contact with the Mg alloy. The material near the keyhole of steel plate undergoes severe plastic deformation. In the subsequent welding heat cycle, dynamic recrystallization was occurred and the grain is refined in this area, which results in the hardness reaching 322 HV. The most obvious feature is that the interface between magnesium and steel presents the shape of "hook". This is due to the stirring action of the pin, and the severe plastic deformation was occurred at the interface. Some steel is embedded into Mg alloy as the form of "rivet", which forms the mechanical bond between Mg and steel in the welded joint. Fig. 19 b–e show all cross-section hardness distribution of the stirring zone, they have similar hardness distribution characteristics. But it can be clearly seen that more "hook" or "rivet" shaped bumps are formed, which proves that Mg and steel undergo a more severe and unstable plastic deformation process. The hardness of some small areas reached over 300 HV, which was due to the direct contact and friction between the stirring tool and the steel during the welding process. The abrasion of the stir-
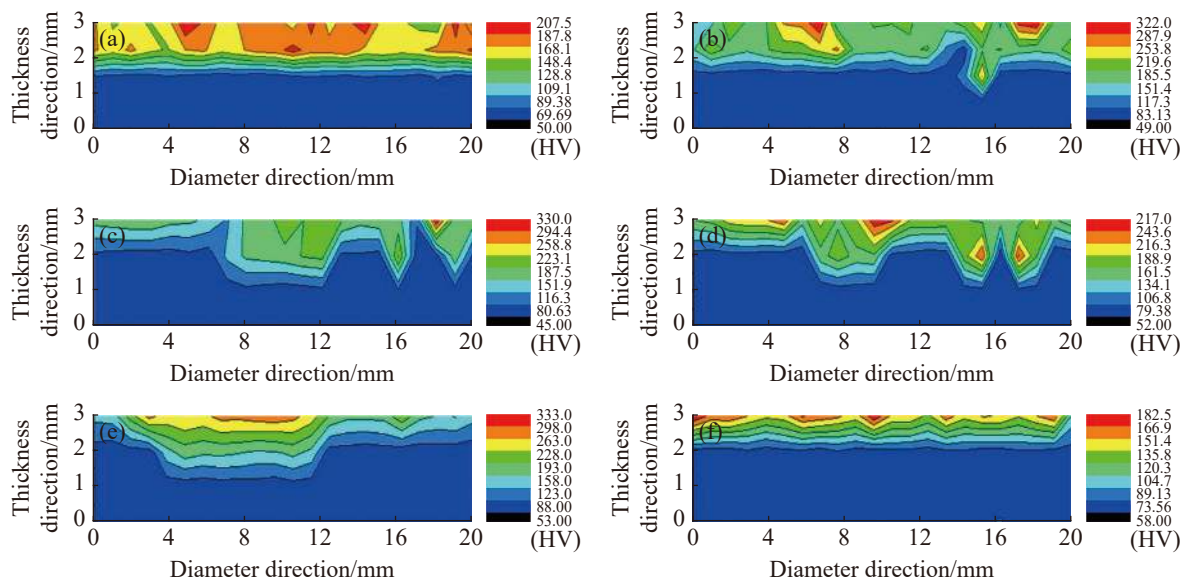
Fig. 19 **Microhardness diagram of cross-section (a) Section A-A (b) Section B-B (c) Section C-C (d) Section D-D (e) Section E-E (f) Section F-F**

ring tool was inevitable. Some shoulder material was adhered to the surface of the welding joint, and even some parts were stirred into the steel matrix, resulting in high hardness in some areas.

2.5 Analysis of in-situ tensile test

Fig. 20 shows the fracture process during in-situ tensile test. After the load is applied on the specimen, the crack source firstly is formed in the shoulder zone near the edge of the welding joint, and then the crack passes through the shoulder zone along the edge of the welding joint and continues to extend to the stirring zone, as shown in Fig. 20 a. The crack extends rapidly in the shoulder zone. When the crack extends to the stirring zone, it is blocked by the solid mechanical/metallurgical bonding zone between Mg and steel. At this time, the crack extends at a significantly lower speed, or even no longer extends for a period of time, as shown in Fig. 20 b and c. As the load continues to increase, the direction of crack extension changes. Crack no longer propagates along the interface between Mg alloy and steel, but along the defective part of Mg alloy or the area of brittle phases in the stirring zone. Crack propagates in the direc-
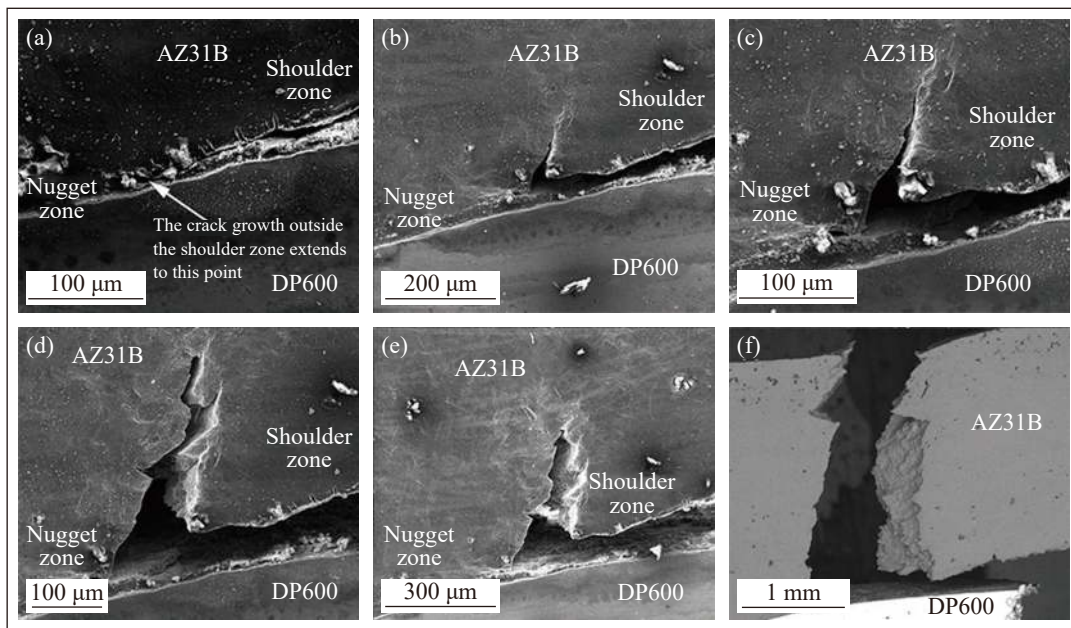
Fig. 20 **Fracture process during in-situ tensile test**

tion perpendicular to the interface between Mg alloy and steel, as shown in Fig. 20 d and e, until the Mg alloy plate is completely broken, as shown in Fig. 20 f.

3   Conclusions

(1) With the measure data and non-destructive method, the three-dimensional entity morphologies of bonding interface were restored by software, which has a better objectivity and accuracy compared with data simulation.

(2) The hardness distribution in the stirring zone is extremely uneven. Due to the severe stirring effect of the stirring pin, some hooks were formed and the hardness of the center was higher than that of the boundary. Some of these hooks are located in the steel matrix, while others are embedded in the Mg alloy matrix. The reason that hook's hardness is higher than that of the steel base metal is that it is subjected to the intense thermal action of the stirring tool. This results in plastic flow and migration, and the grain is broken and refined. It is worth noting that, for the steel hook inserted into the Mg alloy matrix, the grain refining zone greatly improves the mechanical bonding strength of the joint.

(3) The bonding interface of joint between AZ31B Mg alloy and DP600 steel by KFSSW existed a large number of wavy and deformed nail structures that make Mg and steel inosculate each other to form joint with obvious mechanical bonding characteristics. The plastics deformation of metal at the bonding interface mainly occurred in the stirring zone of pin. In other words, the mechanical bonding of the joint mainly existed in the stirring zone. This result can be proved by microhardness and in-situ tensile test analysis.

(4) In this paper, the entity cross-section morphology can objectively reflect the characteristics of the welding process in each stage. It is proved that the interface reproduction method has considerable accuracy and universal applicability.

References

［1］ Yang Z , Li J P and Zhang J X et al. Review on research and development of magnesium alloys. Acta Metallurgica Sinica (English Letters), 2008.

［2］ Sato Y S, Park S, Michiuchi M, et al. Constitutional liquation during dissimilar friction stir welding of Al and Mg alloys. Scripta Materialia, 2004.

［3］ Somasekharan A C, Murr L E. Microstructures in friction-stir welded dissimilar magnesium alloys and magnesium alloys to 6061-T6 aluminum alloy. Materials Characterization, 2004, 52(1):49 − 64.

［4］ Liu L M, Shen Y, Zhang Z D. et al. Effect of cadmium chloride flux in GTA welding of magnesium alloys. Science & Technology of Welding & Joining, 2006.

［5］ Liu X, Wang X J, Wang B S, et al. The role of mechanical connection during friction stir keyholeless spot welding joints of dissimilar materials. Metals - Open Access Metallurgy Journal, 2017, 7(6):217.

［6］ Casalino G, Guglielmi P, Lorusso V D, et al. Laser offset welding of AZ31B magnesium alloy to 316 stainless steel. Journal of Materials Processing Technology, 2016, 242: 49–59.

［7］ Wei Y, Li J, Xiong J, et al. Microstructures and mechanical properties of magnesium alloy and stainless steel weld-joint made by friction stir lap welding. Materials & Design, 2012, 33(1):111 − 114.

［8］ Chen Y C, Nakata K. Effect of surface states of steel on microstructure and mechanical properties of lap joints of magnesium alloy and steel by friction stir welding. Science & Technology of Welding & Joining, 2013, 15(4):293 − 298.

［9］ Chen Y C, Nakata K. Effect of tool geometry on microstructure and mechanical properties of friction stir lap welded magnesium alloy and steel. Materials & Design, 2009, 30(9):3913 − 3919.

［10］ Jana S, Hovanski Y, Grant G J. Friction stir lap welding of magnesium alloy to steel: A preliminary investigation. Metallurgical & Materials Transactions A, 2010, 41(12): 3173 − 3182.

［11］ Abe Y, Watanabe T, Tanabe H, et al. Dissimilar metal joining of magnesium alloy to steel by FSW. Advanced Materials Research, 2007, 15–17:393 − 397.

［12］ Watanabe T, Kagiya K, Yanagisawa A, et al. Solid state welding of steel and magnesium alloy using a rotating pin-solid state welding of dissimilar metals using a rotating pin (Report 3). Quarterly Journal of the Japan Welding Society, 2006, 24(1):108 − 115.

［13］ Carrino L, Squillace A, Paradiso V, et al. Superplastic forming of friction stir processed magnesium alloys for aeronautical applications: a modeling approach. Materials Science Forum, 2013, 735:180 − 191.

［14］ Shen A Z, Chen B Y, Haghshenas M, et al. Role of welding parameters on interfacial bonding in dissimilar steel/aluminum friction stir welds. Engineering Science and Technology, an International Journal, 2015, 18(2):270 − 277.

［15］ Chiteka K. friction stir welding of steels: areview paper. 2017.

［16］ Wang X, Zhao G, Zhang Z, et al. Process research on friction stir spot welding without key hole between magnesium and steel dissimilar alloys. Hot Working Technology, 2012.

［17］ Zhang Z K, Wang X J, Wang P C, et al. Friction stir keyholeless spot welding of AZ31 Mg alloy-mild steel. Transactions of Nonferrous Metals Society of China, 2014, 24(6):1709 − 1716.

［18］ Lü Zongliang, Han Zhenyu, Zhu Dong, et al. Enlarged-end tool for friction stir lap welding towards hook defect controlling. China welding, 2020, 29(1):1 − 7.